VIBRATION AND STABILITY OF AXIALLY MOVING WEBS COUPLED TO SURROUNDING AIR

by

M. D. Vaughan and A. Raman
Purdue University
USA

ABSTRACT

High-speed web flutter is of significant importance in a variety of paper, plastics, textiles, and sheet metal industries. The natural frequencies of vibration and the onset of flutter in thin, wide, high-speed webs are investigated by modeling a web as an axially moving, partially slack Kirchhoff plate with small bending stiffness, and coupled with surrounding air. The linear partial differential equations of the web are discretized using the Assumed Modes Method and analyzed for two different air models – incompressible and compressible flow. The solutions for the aerodynamic potentials are determined numerically and accurate reduced order models of the moving web with air coupling are generated.

In the absence of air coupling the web frequencies are grouped together in clusters and aeroelastic flutter occurs at supercritical speed. Addition of incompressible potential flow air coupling reduces significantly the web frequencies and separates the frequency clusters while modifying slightly the onset and frequency of flutter at supercritical speed. Compressible flow modeling adds radiation damping to the system and shifts the onset of flutter to the critical speed. Finally it is concluded that the prediction of web flutter at subcritical speeds requires the inclusion of base flows generated by air viscosity and web motion. These results corroborate previous results in the literature and suggest systematic analytical modeling approaches for web flutter prediction.

NOMENCLATURE

a	Length of web span	C	Amplitude of mass normalized eigenfunctions
b	Width of web		
c	Web transport speed		

D	Web bending stiffness, $D = E \quad h^3/12 \quad (1-\mu^2)$
E	Young's modulus of the web material
f	Forcing function
h	Web thickness
N_{xx}	Membrane normal force/length along X
N_{xy}	In-plane membrane shear force/length
N_{yy}	Membrane normal force/length along Y
p	Aerodynamic pressure difference on the web
u	Eulerian description of transverse web deflection
α, γ	Variables describing the cross-span mode shapes
ε	Bending stiffness to tension ratio, $\varepsilon = D/a^2 N_{xx}$
ϕ	Aerodynamic potential
κ	Web aspect ratio, b/a
λ	System eigenvalue
μ	Web Poisson's ratio
ρ	Web mass per unit area
ρ_{air}	Air density
ω	Web natural frequency
ψ_{mn}	Basis function for discretization
Λ	Web density parameter, $\Lambda = a\rho_{air}/\rho$
∇^4	Biharmonic operator

INTRODUCTION

The manufacture, processing, and use of paper, plastics, magnetic tapes, thin sheet metals, and textiles often involves high speed transport of thin, wide continuous sheets of material known as webs. Tension is applied to the web in the direction of its transport as it travels through a series of rollers, while its edges remain unsupported. High amplitude web vibration, characterized as flutter, has been observed at the free edges. Flutter leads to poor quality products and even web breakages, causing large financial losses.

The problem of web flutter is part of the study axially moving materials. Webs, elevator cables, tramway cables, band saws, chains and bands, and pipes conveying fluid have been studied in this context (see for example, the review article by Wickert and Mote [1]). The axial transport generates additional particle acceleration terms in the equations of motion rendering gyroscopic the system dynamics. This makes the problem similar to rotating machinery like hard disk drives or circular blades. The present work, however, focuses on the stability of a thin, wide, axially moving plate with a small but finite bending stiffness to tension ratio coupled to the surrounding air.

The transverse vibrations of wide axially moving media in the absence of fluid coupling have been studied through the use of pre-stressed moving plate models, and linear and nonlinear membrane models. Ulsoy and Mote [2] used the classical Ritz discretization of a pre-tensioned axially moving plate to study the vibrations of wide bandsaw blades. Wang [3] developed a mixed finite element formulation based on Mindlin-Reissner plate theory with transverse deflection and shear deformation included in order to predict stresses in orthotropic webs. Laukkanen [4] extends the work by Wang [3] by offering a correction to the gyroscopic inertia matrix and illustrating how waves reflect

at the free edges in the given model. Although normal pressures due to air loading may be implemented in the FEM formulations described above, the pressure loading is an input to the equations, and therefore must be assumed or known *a priori.* Koivurova and Pramila [5] included geometric nonlinear effects modeling the vibrations of a membrane and showed that critical speed increased slightly. Mockensturm and Mote [6] investigated steady motions of translating twisted webs via a non-linear shell theory. They showed that any degree of twist at sub-critical speeds causes increased compressive stresses in the free-free direction, increasing the likelihood of wrinkling.

The vibrations and flutter of *stationary* webs and thin films coupled to a surrounding moving fluid have been studied by a number of investigators. Guo and Paidoussis [7] investigated the stability of a rectangular plate in channel flow, modeling the plate as a beam in a potential flow. However width dependent effects were neglected in the model. Web flutter observations in moving webs have demonstrated that flows induced in the cross machine direction can cause web flutter. Blowers in drying processes may introduce this type of flow. Motivated by this observation, several researchers have studied the vibrations and stability of stationary webs with various boundary conditions and subject to a cross fluid flow. Chang and Moretti [8] and Chang, Cho, and Moretti [9] modeled the web as a half infinite, tensioned, translating Kirchhoff plate surrounded a potential flow field with a base velocity in the cross machine direction. Chang and Moretti [10] include a translating web in the initial model but neglect its effect in the subsequent analyses. These papers present several experiments on stationary and moving webs in a cross flow. The critical cross flow speed generally tended to increase with increasing tension, while the effect of the transport velocity was unclear in the range of velocities tested (0 to 4.88 m/s). Further, the theoretical critical speed was generally less than the measured critical speed, but not in all cases. Watanabe, Suzuki, Sugihara, and Sueoka [11] also investigated flutter due to cross flow on paper sheets supported only at the leading edge and on stationary paper webs. Thin sheets (0.028mm) were noted to exhibit complicated motion that included cross flow directional modes while thick paper (0.235mm) exhibited a simpler motion that the authors described as traveling waves moving in the flow direction. Photography of smoke streamlines demonstrates that there is no large-scale flow separation around fluttering sheets or webs. Although vortices tend to be more abundant around the thinner sheet tested, they are small and thus irrotational flow may be assumed. Watanabe, Isogai, Suzuki, and Sugihara [12] used a beam model and estimated the unsteady lift and friction drag on a web to predict the onset of flutter due to cross flow. Their model also under predicted the cross flow flutter speed.

The coupling of *traveling* webs with surrounding air has for the most part been investigated using one dimensional beam or string models along with ad hoc fluid models. Pramila [13, 14] showed that the effective mass of the web is increased because of the surrounding air. In both works the effect of the added mass on the web critical speed was investigated. In both cases the stationary fundamental frequency of the web is reduced by as much as 400% due the added inertia effect from the air. Pramila [13, 14] experimentally verified the reduced frequencies on a web moving at low sub-critical speeds. Wang [15] investigated the effect of web porosity and dual sided air bearings on the traveling string with added mass model. His results demonstrated that air bearings tend to reduce the amplitude of oscillations and that web porosity has very little effect on transient response for the scenario considered.

To refine the inclusion of fluid coupling Niemi and Pramila [16] performed a FEM analysis of a linear membrane submerged in an initially quiescent potential, incompressible flow. The results demonstrated that the web frequencies reduce without affecting the onset of critical speed. However, a uniaxially tensioned linear web model is a fundamentally ill-posed problem. To avoid this problem they had to introduce an artificial tensioning effect in the cross-span direction. Clearly therefore web vibration models are best posed naturally as uniaxially tensioned plates with very small bending stiffness or as nonlinear membranes.

Raman, Wolf, and Hagedorn [17] modeled a continuous web supported between rollers as a thin axially moving Kirchhoff plate with small but finite bending stiffness to tension ratio. The effects of air coupling and non-uniform tension were included in the model. However, the focus of the paper was on the frequency clustering effects in paper webs. For each mode shape in the tensioned direction several cross-span mode frequencies with nearly identical frequencies cluster together. Forced vibrations near a particular frequency will include several modes in each cluster, the combination of which can result in edge flutter. Experiments on a stationary web demonstrated the existence of frequency clusters. Numerical results on the fluid coupling were not presented.

The present work extends the work of Raman, Wolf, and Hagedorn [17] to investigate in detail the effects of the fluid coupling on the web vibration and stability at sub- and supercritical speeds. Further, results from both incompressible and compressible fluid coupling are compared.

MODELING

The rectangular web considered here is modeled as an isotropic linear elastic axially moving Kirchhoff plate. The equations of motion describing the transverse vibrations of such a plate were derived by Ulsoy and Mote [2] using Hamilton's principle and are given as

$$\rho u_{,tt} + 2\rho c u_{,xt} + \rho c^2 u_{,xx} + D\nabla^4 u - (N_{xx}u_{,xx} + 2N_{xy}u_{,xy} + N_{yy}u_{,yy}) = f \qquad (1)$$

with the variables defined in the nomenclature section above. The web is uniaxially tensioned in the X direction ($N_{xx} \neq 0$, $N_{xy} = 0$, $N_{yy} = 0$) and translating along the X axis with constant velocity c. The web is free at $y = -b/2,\ b/2$ and is assumed to be simply supported at the upstream and downstream edges, $x = -a/2, a/2$, respectively. See Figure 1. Simply supported boundary conditions are a suitably accurate boundary condition for predicting the linear vibrations of webs with small bending stiffness to tension ratio stretched across finite radius rollers (Turnbull *et al.* [18]).

The aerodynamic coupling of the web with surrounding air is also considered. An aerodynamic potential $\phi(x, y, z, t)$ is defined throughout the fluid domain. The pressure on the web $p(x, y, t)$ is the difference of aerodynamic pressure on the bottom and upper face of the web can be written as (Niemi and Pramila [16])

$$f = p(x,y,t) = 2\rho_{air}\phi_{,t}(x,y,0^{+},t) \tag{2}$$

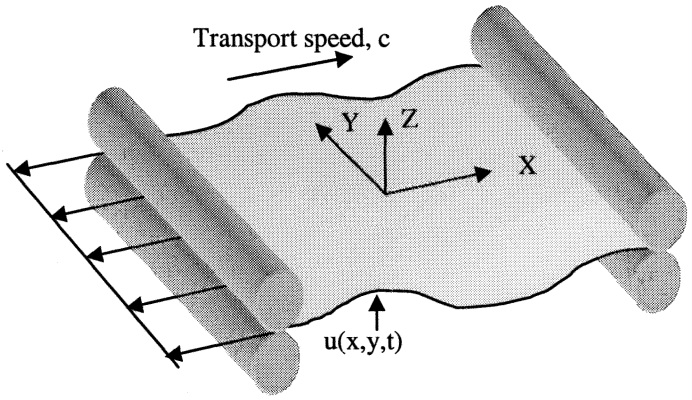

Figure 1. Schematic of the translating web system with uniform uniaxial tension and aerodynamic coupling

Further, the inviscid flow assumption requires that the normal fluid velocity on the web equal the local component of transverse velocity at a point. The following quantities are introduced to non-dimensionalize the system (Raman, *et al* [17]):

$$u' = u/a,\ x' = x/a,\ y' = y/a,\ z' = z/a$$

$$D = \frac{Eh^3}{12(1-\mu^2)},\ \varepsilon = \frac{D}{a^2 N_{xx}},\ t' = \frac{1}{a}\sqrt{\frac{N_{xx}}{\rho}}t,\ N'_{xx} = \frac{N_{xx}}{N_{xx}} = 1,\ \kappa = \frac{b}{a} \tag{3}$$

$$\Lambda = \frac{a\rho_{air}}{\rho},\ c' = \frac{c}{\sqrt{N_{xx}/\rho}},\ \phi'(x',y',z',t') = \phi(x,y,z,t)\ \ a\sqrt{\frac{N_{xx}}{\rho}}$$

The primes denote the dimensionless quantities and are dropped in the subsequent analysis. In the nondimensionalized variables, $\mathcal{A} = \{(x,y)\,|\,-1/2 < x < 1/2,\ -\kappa/2 < y < \kappa/2\}$ is the area of the web in the span. Appending the surrounding fluid pressure to the equations of motion of a flat, translating plate, (Ulsoy and Mote [2]), the equations of motion and fluid continuity equations of the surrounding incompressible fluid can be written as

$$\begin{aligned} &\varepsilon\nabla^4 u + u_{,tt} + 2cu_{,xt} + (c^2-1)u_{,xx} = 2\Lambda\phi_{,t}(x,y,0^{+},t) \quad \text{on } \mathcal{A} \\ &\nabla^2\phi = 0 \quad \text{in } \mathcal{R}^3 \setminus \mathcal{A} \end{aligned} \tag{4}$$

The corresponding boundary conditions are

$$u(-1/2,y,t)=u(1/2,y,t)=0,\ u_{,xx}(-1/2,y,t)=u_{,xx}(1/2,y,t)=0$$

(simply supported at x = −1/2,1/2)

$$u_{,yy}(x,-\kappa/2,t)+\mu\ u_{,xx}(x,-\kappa/2,t)=u_{,yy}(x,+\kappa/2,t)+\mu\ u_{,xx}(x,+\kappa/2,t)=0$$

$$u_{,yyy}(x,-\kappa/2,t)+(2-\mu)\ u_{,yxx}(x,-\kappa/2,t)=u_{,yyy}(x,+\kappa/2,t)+(2-\mu)\ u_{,yxx}(x,+\kappa/2,t)=0$$

(free edges at $y=-\kappa/2,\ \kappa/2$)

$$\phi_{,z}(x,y,0^{+},t)=u_{,t}\quad \text{on}\quad \mathcal{A}\ \text{(velocity matching)}$$

$$\lim_{r^2\to\infty}\phi_{,n}(x,y,z,t)=0,\ \text{where}\ r^2=x^2+y^2+z^2\ \text{(farfield radiation condition)}\quad (5)$$

$$\phi(x,y,0^{+},t)=0\quad \text{outside}\quad \mathcal{A}\ \text{(unbaffled web)}$$

The equations of motion (4) are discretized using the Assumed Modes Method method. The mass-normalized eigenfunctions, $\psi_{mn}(x,y)$ of a uniformly tensioned, stationary web $(c=0)$ and without aerodynamic coupling $(\Lambda=0)$ are used as basis functions for the discretization of (4). The discretization is performed in the configuration space formulation of the gyroscopic eigenvalue problem. Accordingly

$$\begin{aligned}
&u(x,y,t)=\sum_{m=0}^{\infty}\sum_{n=0}^{\infty}q_{mn}(t)\quad \psi_{mn}(x,y)\\
&\psi_{mn}(x,y)=C_{mn}X_m(x)Y_{mn}(y)\\
&X_m(x)=\sin((m+1)\pi x)\\
&Y_{mn}(y)=\cosh(\alpha_{mn_1}y)+\gamma_{mn}\cosh(\alpha_{mn_2}y)\qquad n=0,2,4...\\
&Y_{mn}(y)=\sinh(\alpha_{mn_1}y)+\gamma_{mn}\sinh(\alpha_{mn_2}y)\qquad n=1,3,5...
\end{aligned}\quad (6)$$

where the basis functions $\psi_{mn}(x,y)$ possess m nodes along the X axis and n nodes along the Y axis. The variables α,γ that describe the cross-span mode shapes are found by solving the characteristic equation formed from the boundary conditions of the web. Note that the basis functions can be divided conveniently into those that are symmetric or antisymmetric in the cross-span direction. The lowest frequency mode at zero speed has zero nodal lines in each direction and is symmetric across both axes. Further the aerodynamic potential is also expanded as follows

$$\phi(x,y,z,t)=\sum_{m=0}^{\infty}\sum_{n=0}^{\infty}A_{mn}(t)\quad \varphi_{mn}(x,y,z)\quad (7)$$

Substitution of the expansions into the velocity matching boundary condition (5) and the separation of time and spatial variables leads to

$$A_{mn}(t) = -\dot{q}_{mn}(t)$$
$$\varphi_{mn,z}(x,y,0^+) = -\psi_{mn}(x,y) \quad \text{on} \quad \mathcal{A} \tag{8}$$
$$\varphi_{mn}\ (x,y,0^+) = 0 \quad \text{outside} \quad \mathcal{A}$$

with the other boundary conditions for $\varphi_{mn}(x,y,z)$ adjusted from (5). Thus for a given mode mn the pressure loading is given as

$$p_{mn}(x,y,t) = -2\Lambda\varphi_{mn}(x,y,0^+)\ddot{q}_{mn}(t) \tag{9}$$

Because the pressure loading is a function of the second time derivative of web modal coordinates, the fluid adds inertia to the web system. A baffled web assumption precludes any exchange of the surrounding fluid between the upper and lower half spaces leading to larger estimates of the added fluid inertia effect. However, an unbaffled web assumption allows for exchange of fluid between the upper and lower half spaces thus modeling correctly the fluid motion near the free edges of the web. This leads to a mixed boundary value problem at $z = 0$ consisting of a Neumann boundary condition on $\mathcal{A}$ and a Dirichlet boundary condition outside $\mathcal{A}$. In this article a finite element model (FEM) of the incompressible fluid is used to compute the pressure loading for each basis function.

For the Assumed Modes Method, consider a N term expansion in equations (6) and (7). Substitution of these expansions into the kinetic and strain energy functions and the use of Langrange's equations of motion for conservative systems lead to a set of discretized ordinary differential equations. The results will be the same as those derived from the Rayleigh-Ritz method when the energy form of Rayleigh's quotient is used [19]. This leads to the following discretized equations of motion:

$$(\mathbf{I} + 2\Lambda\ \mathbf{M_{air}})\ \ddot{\mathbf{q}} + 2c\ \mathbf{G}\dot{\mathbf{q}} + (1-c^2)\mathbf{K}_1\mathbf{q} + \varepsilon\ \mathbf{K}_2\ \mathbf{q} = \mathbf{0} \tag{10}$$

where $\mathbf{I}$ is the $N \times N$ identity matrix, and

$$(M_{air})_{ij\,;\,mn} = \int_{x=0}^{1}\int_{y=-\kappa/2}^{+\kappa/2} \varphi_{mn}(x,y,0^+)\ \psi_{mn}(x,y)\ dx\ dy$$

$$(G)_{ij\,;\,mn} = \int_{x=0}^{1}\int_{y=-\kappa/2}^{+\kappa/2} \psi_{ij}(x,y)\ \ (\psi_{mn}(x,y))_{,x}\ dx\ dy$$

$$(K_1)_{ij\,;\,mn} = -\int_{x=0}^{1}\int_{y=-\kappa/2}^{+\kappa/2} (\psi_{ij}(x,y))_{,x}\ \ (\psi_{mn}(x,y))_{,x}\ dx\ dy \tag{11}$$

$$\begin{aligned}(K_2)_{ij\,;\,mn} = \int_{x=0}^{1}\int_{y=-\kappa/2}^{+\kappa/2} \{&(\psi_{mn}(x,y))_{,xx}(\psi_{ij}(x,y))_{,xx} + (\psi_{mn}(x,y))_{,yy}(\psi_{ij}(x,y))_{,yy} \\ &+2(1-\mu)(\psi_{mn}(x,y))_{,xy}(\psi_{ij}(x,y))_{,xy} \\ &+\mu[(\psi_{mn}(x,y))_{,xx}(\psi_{ij}(x,y))_{,yy} + (\psi_{mn}(x,y))_{,yy}(\psi_{ij}(x,y))_{,xx}]\}dx\ \ dy\end{aligned}$$

$\mathbf{q}(t)$ is the vector of the generalized coordinates $q_{mn}(t)$ and $\mathbf{M_{air}}$ is the symmetric aerodynamic loading matrix (usually non-diagonal). $\varphi_{mn}(x, y, 0^+)$ is the aerodynamic potential at the web surface solved with the FEM. $\mathbf{G}$ is the skew-symmetric gyroscopic matrix, while $\mathbf{K_1}$ is the diagonal stiffness matrix due to the tension. The diagonal entries of $\mathbf{K_1}$ are the squares of the natural frequencies of an equivalently tensioned string i.e. $\pi^2, (2\pi)^2$ and so on. $\mathbf{K_3}$ is the symmetric bending stiffness matrix.

Several key parameters appear in the discretized equations (11): Λ, c, and ε. These represent respectively, the ratio of air density to web density, the non-dimensional transport speed, and the web stiffness to applied tension ratio. The effect of the air loading and the speed on the web stability will also be discussed. Note that no aerodynamic or viscoelastic damping has been included in the model. In what follows, first the details of the finite element method are discussed followed by an investigation of convergence issues in the proposed computational scheme.

FEM FOR THE FLUID DOMAIN

The objective of the finite element discretization of the fluid domain is to evaluate the added mass matrix (equation (10)) of the discretized web model. The use of the stationary, in-vacuo web basis functions facilitates greatly this computation. Indeed all that remains to be computed for the evaluating the added mass matrix is the aerodynamic potential $\varphi_{mn}(x, y, z)$ generated in the fluid domain by the oscillation of the web in its $\psi_{mn}(x, y)$ mode. From this, the quantity $\varphi_{mn}(x, y, 0^+)$ and the matrix $\mathbf{M_{air}}$ can be evaluated easily.

Only 1/4 of the semi-infinite fluid domain need be considered due to the nature of the loading (see Figure 2). The infinite boundary is truncated to a finite radius r. However the boundary conditions on the XZ and the YZ planes depend on the basis function $\psi_{mn}(x, y)$ used in the computation. With the X and Y axes centered on the web the YZ is a plane of symmetry for modes that are symmetric in the in-span direction, and it is a plane of anti-symmetry for modes that are antisymmetric in the in-span direction. The result is similar for the XZ plane and cross-span direction. On planes of symmetry the normal velocity is set to 0, while on planes of anti-symmetry $\varphi_{mn}(x, y, z) = 0$. Accordingly

$$\varphi_{mn,n}(x,y,z) = 0 \quad \text{at } \varphi_{mn} = r$$

$$\varphi_{mn,x}(0,y,z) = 0 \text{ for in-span symmetric modes}$$

$$\varphi_{mn}(0,y,z) = 0 \text{ for in-span anti-symmetric modes}$$

$$\varphi_{mn,y}(x,0,z) = 0 \text{ for cross-span symmetric modes}$$

$$\varphi_{mn}(x,0,z) = 0 \text{ for cross-span anti-symmetric modes}$$

$$\varphi_{mn,z}(x,y,0^+) = -\psi_{mn}(x,y) \quad \text{on} \quad \mathcal{A}$$

$$\varphi_{mn}(x,y,0^+) = 0 \quad \text{off} \quad \mathcal{A}$$

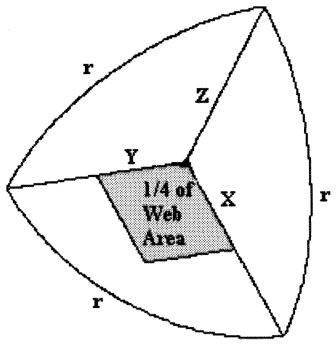

Figure 2. Schematic of Finite Element Model with Boundary Conditions.
The coordinate system origin is near the viewer.

ANSYS steady-state thermal analysis (for Poisson's equation) with solid 20 noded 3D brick elements was used for the computation. Velocity gradients are higher near the web, especially at the free edges, necessitating the use of a very fine mesh there. A fine mesh is used on the web surface area and just above it and the overall mesh is graded with over 85% of the total nodes placed within one half unit of the web surface. To ensure accuracy in this preliminary study approximately 80 000 nodes were used. The solutions were loaded into MATLAB to take inner products with respect to the mode shapes to evaluate the components of the matrix $\mathbf{M}_{\mathbf{air}}$.

To analyze the effect of the finite fluid domain approximation in the FEM, a detailed analysis of the effects of the fluid domain size r on the added mass matrix was performed. The fluid finite element domain needs to be large enough to approximate the infinite radius domain. Table 1 describes the variation with r/κ of the added mass matrix components of the $\psi_{00}, \psi_{01}, \psi_{10}$ basis functions. The table indicates that the added mass components converge rapidly within 4 significant figures with increasing r/κ for ψ_{01}, ψ_{10} basis functions. This convergence is somewhat slower for the fundamental in-vacuo mode ψ_{00}. Accordingly, an appropriate r/κ ratio of 10 is used for the subsequent computation.

r/κ	$\int_{\mathcal{A}} \varphi_{00}\psi_{00}\, d\mathcal{A}$	$\int_{\mathcal{A}} \varphi_{10}\psi_{10}\, d\mathcal{A}$	$\int_{\mathcal{A}} \varphi_{01}\psi_{01}\, d\mathcal{A}$
1	0.2598	0.1420	0.0835
2	0.2426	0.1410	0.0834
4	0.2407	0.1410	0.0834
6	0.2405	0.1410	0.0834
8	0.2404	0.1409	0.0834

Table 1. Terms along the diagonal of the $\mathbf{M}_{\mathbf{air}}$ matrix.

The method used here to calculate the aerodynamic pressure loading on the web is similar to the method presented by Niemi and Pramila in [16], although several aspects of the solution method here are significantly different than that of [16]. Niemi and Pramila model the web as a tensioned translating linear membrane unbaffled at the free edges but with infinite vertical baffles to model the rollers at the fixed edges. A uniaxially tensioned linear membrane model is a fundamentally ill-posed problem so Niemi and Pramila introduced a small artificial tension in the cross span direction. The work here models the web as a tensioned translating plate surrounded by a completely unbaffled incompressible fluid. Niemi and Pramila use finite elements to discretize the moving membrane equation of motion. Here stationary tensioned plate mode shapes and the Assumed Modes Method are used to discretize the tensioned translating plate EOM. Also included here is a discussion of the web stability behavior at super-critical speeds, the motion of the fluid near the web edges, and the effect of fluid compressibility.

CONVERGENCE ISSUES

The number of modes used in the Assumed Modes Discretization needs to be sufficient to correctly predict the stability of the web system with different parameters. The calculated system frequencies will be exactly accurate at zero speed and highly accurate at low speeds regardless of the number of modes used because the stationary tensioned plate mode shapes are the basis functions for the discretization. However to correctly predict eigenvalues at supercritical speeds more basis functions need to be included than those that are to be analyzed subsequently.

Figure 3 shows the convergence behavior of the 00 and 10 modal frequencies at $c = 1.0027$ and the convergence behavior of the 01 and 11 modal frequencies at $c = 1.00354$. The first 2 approximations of the 11 modal frequency are off the scale. For the given speeds the 00 and 01 modes have undergone divergence instability at lower speeds but are gyroscopically stabilized here and they converge to their true solutions monotonically from below. The 10 and 11 modes have not yet undergone divergence instability and they converge to their true solutions monotonically from above. Dual mode flutter (mode 00 with mode 10; mode 01 with mode 11) will occur with a slight increase in speed. The approximations are poor with 2 or 3 clusters in the discretization, but are good and change very little with 4 or more clusters in the discretization. Thus to accurately predict the frequencies of the $m = 0$ and $m = 1$ in-span frequency cluster at least 4 mode shape clusters are needed. This can be generalized to the use of $2(m+1)$ clusters to predict the m^{th} and below cluster

frequencies. Increasing the number of cross-span modes per cluster has little effect on the system convergence. In this paper 6 clusters with 4 cross-span modes each are used for the discretization, with only the first 3 clusters (m = 0, 1, 2) analyzed in the results.

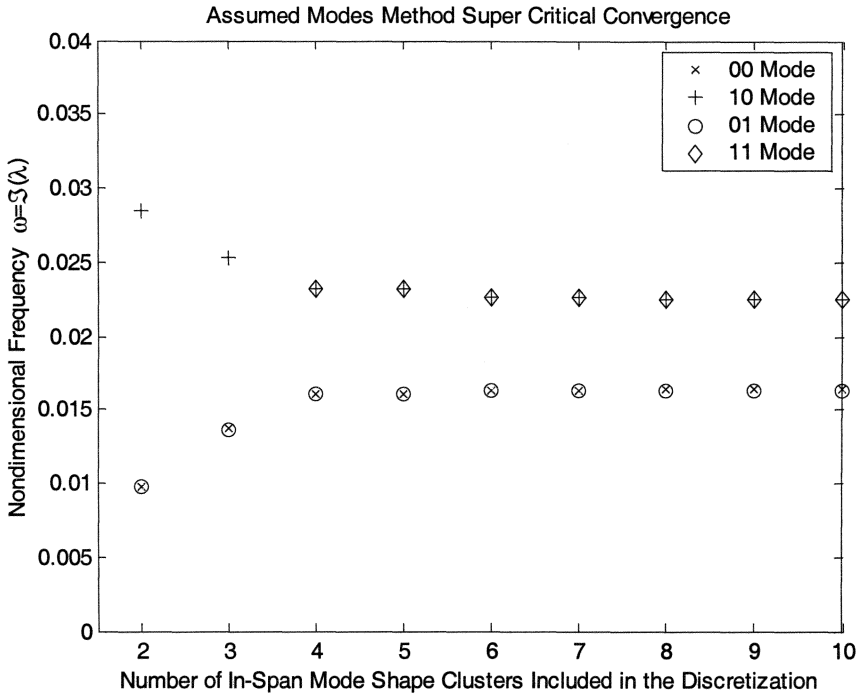

Figure 3. Convergence of approximated frequency solutions to real solutions as the number of in-span mode clusters is increased. Four cross-span modes are included in each cluster. Symmetric cross span modes 00 (x) and 10 (+) are calculated at $c = 1.0027$ and anti-symmetric cross span modes 01 (o) and 11 ($\Diamond$) are calculated at $c = 1.00354$.

RESULTS

The properties of the web considered here are listed in Table 2. These web properties yield the following nondimensional parameter values: $\kappa = 1$, $\varepsilon = 10^{-4}$, $\Lambda = 40$. The Young's Modulus and Poisson's Ratio are estimates for paper properties from the literature (see [10]). The length, width, thickness, and areal density of the web are measured properties obtained from a paper web span in a high speed industrial printing press. The web tension from the press was 1000 times the value used in this paper and would correspond to $\varepsilon = 10^{-7}$. The stability results and conclusions for both $\varepsilon = 10^{-4}$ and $\varepsilon = 10^{-7}$ would be the same, the only difference being that divergence, stabilization, and flutter would happen within a much smaller speed range for the smaller value of ε.

Property	a	b	h	E	μ	N_{xx}	ρ	ρ_{air}
Value	1.372	1.372	25.4	6.8	0.3	0.1	40	1.225
Units	m	m	μm	GPa	-	N/m	g/m^2	kg/m^3

Table 2. Properties of web span used in computations, corresponding to $\kappa = 1$, $\varepsilon = 10^{-4}$, $\Lambda = 40$.

Incompressible Flow

Figure 4a shows the 00 basis function (in-vacuo stationary web mode shape) and Figure 4b shows the corresponding aerodynamic potential computed in ANSYS that is developed on the web surface. These fluid potential distributions are used in calculating the $\mathbf{M_{air}}$ matrix. Symmetry and anti-symmetry in the mode shapes (in the cross span direction) are preserved in the corresponding aerodynamic loadings. The fluid velocity at the free edge is shown in Figure 4c and the velocity at the fixed edge is shown in Figure 4d. Just off of the free edge the fluid velocity is high, at least one order of magnitude above the velocity boundary condition imposed on the web surface. The velocity gradients are also very high in the Y direction close to the free edge. Just off of the simply supported edge the velocity is also large, but much smaller than the velocity at the free edge. The high fluid velocity gradients near the free edge underscore the importance of fine mesh refinement near the free edge of the web. Further, the FEM computations clearly demonstrate that fluid mass transport occurs from above to below the web and vice versa near the free web edges. This important effect is ignored by a baffled web assumption.

Without air coupling the web vibration frequencies are clustered tightly together around those of an equivalently tensioned string. Addition of incompressible flow coupling greatly reduces the web vibration frequencies and separates frequencies within a cluster, (See Figure 5). The reduction in frequency is most dramatic in the 00 mode with the stationary air-coupled 00 modal frequency equal to 21% of the uncoupled frequency. The stationary air-coupled 10 modal frequency is reduced to 27% of the uncoupled 10 modal value, and the 12 mode frequency is reduced to 41% of its uncoupled value. The reduction in the 00 mode is corroborated by the previous work of Pramila [13,14,16]. It should be noted however that for an equivalent Λ the effect of air coupling calculated by Niemi and Pramila [16] is slightly larger than the effect calculated here. This is expected since their model included a baffle at the fixed edges and the current model does not. Note however that Niemi and Pramila [16] use diagonalization techniques which are unable to accurately capture the air coupling with the anti-symmetric cross-span modes.

The supercritical speed stability of the in-vacuo web is discussed first. At the first critical speed the in-vacuo web system 00 mode undergoes divergence instability. As the speed is increased is gyroscopically restabilizes until it coalesces with the 10 mode and the system undergoes coupled mode flutter. Both the 00 and 10 modes are symmetric cross-span modes. The behavior is similar for anti-symmetric cross-span modes but at slightly higher speeds. The 01 mode diverges and the 01, 11 modes flutter at a slightly higher speed. As speed increases more modes from different mode clusters diverge, coalesce and flutter (See Figure 6 (a) and (c)).

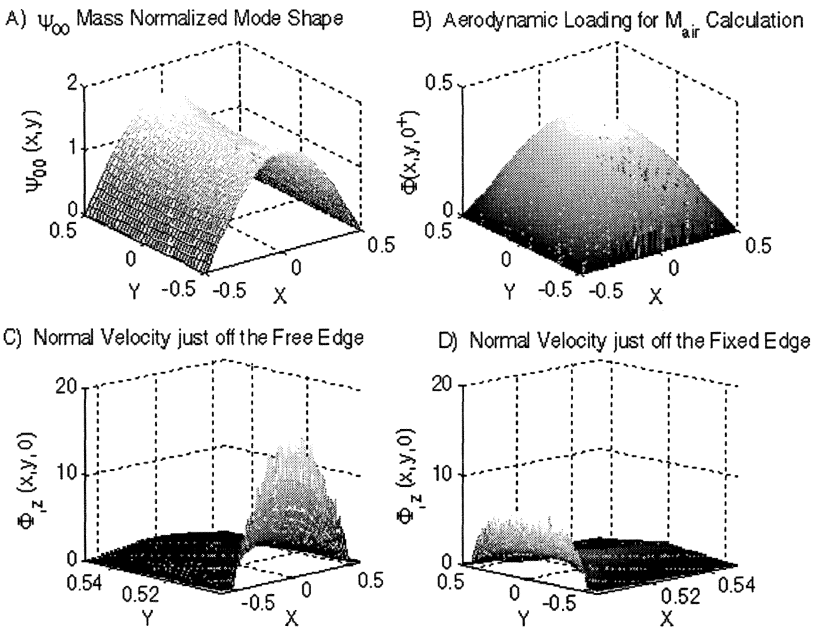

Figure 4. (a) Mass Normalized ψ_{00} basis function, (b) corresponding aerodynamic potential generated at the surface, (c) Normal velocity just off the free edge of the web at $z=0$, (d) Normal velocity just off the fixed edge at $z=0$.

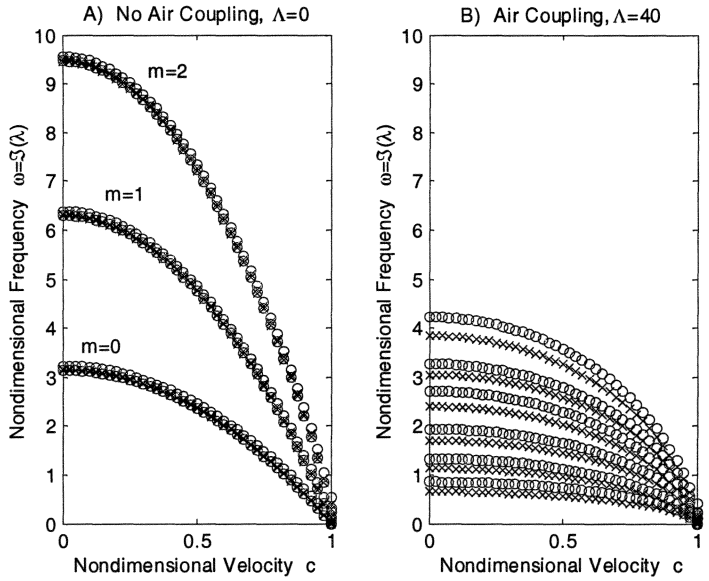

Figure 5. (a) Modal frequencies of the in-vacuo ($\Lambda=0$) web system vs. speed. (b) Modal frequencies of the incompressible air-coupled ($\Lambda=40$) web system. For both plots: symmetric cross-span modes (x), anti-symmetric cross-span modes (o).

Aerodynamic coupling affects subtly the supercritical speed stability (see Figure 6). The system critical speeds remain unchanged. The speeds of gyroscopic stabilization are also unchanged. The flutter speeds and frequencies however are slightly lower compared to the in-vacuo case. The reduction in modal frequencies and flutter onset speeds is more pronounced in higher order modes, as can be seen by comparing the 20 and 21 modes in Figures 6 (a) and (b).

The effect of the parameter Λ on supercritical speed web stability is demonstrated in Figure 7. Critical speeds do not change with Λ. The speed of gyroscopic stabilization and remains unchanged, the speed of the onset of flutter decreases, and modal frequency at the onset of flutter decreases as Λ is increased until a critical value of Λ. At this critical Λ value the speed of the onset of flutter is equal to the speed at which the system had reached gyroscopic stabilization and the flutter frequency vanishes. As Λ is increased above its critical value gyroscopic stabilization no longer occurs, the flutter speed increases and modal frequency at the onset of flutter remains zero. For the web parameters listed in Table 1 the critical Λ values for 00, 10 and 01,11 coupled mode flutter, are respectively 2900 and 3500.

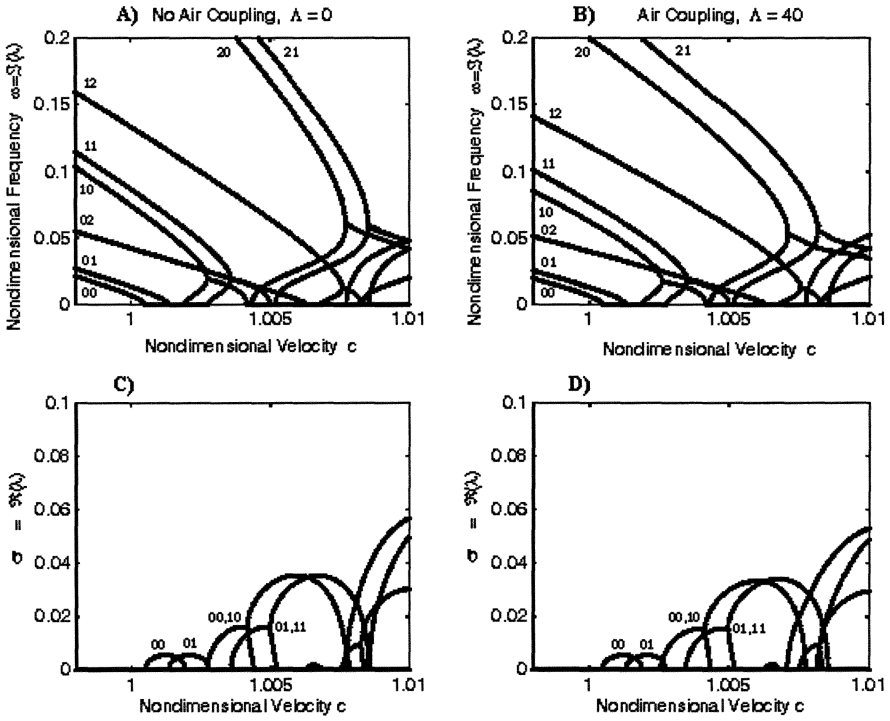

Figure 6. Eigenvalues of the web system just before, at, and after the critical speed, (a) Imaginary part of in-vacuo ($\Lambda = 0$) web system eigenvalues., (b) Imaginary part of incompressible air-coupled ($\Lambda = 40$) web system eigenvalues, (c) Real part of in-vacuo ($\Lambda = 0$) web system eigenvalues., (d) Real part of incompressible air-coupled ($\Lambda = 40$) web system eigenvalues. Mode numbers are labeled on the plot.

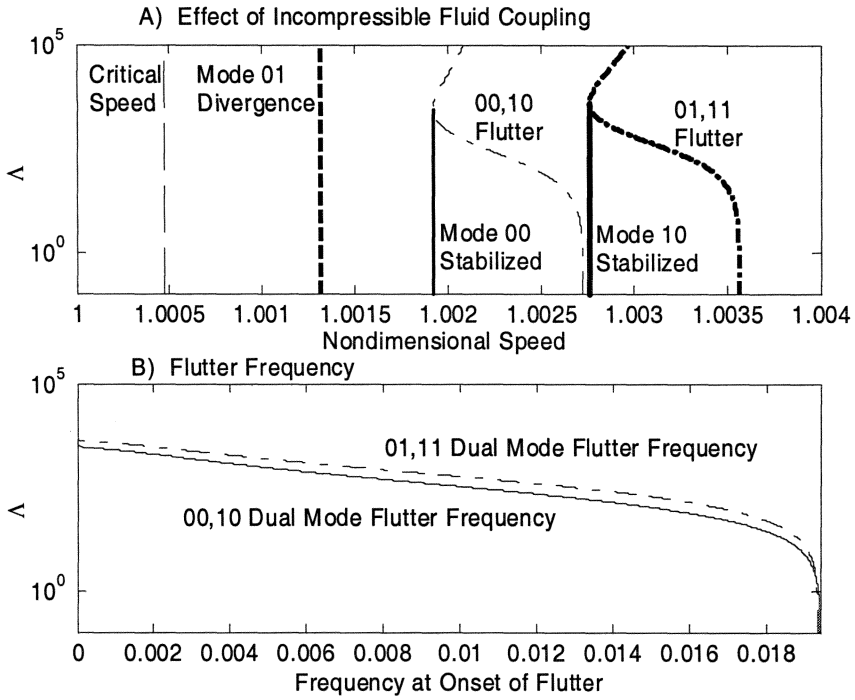

Figure 7. A) Variation in critical speed, speed of gyroscopic stabilization and flutter vs. Λ. B) Variation in modal frequency at the onset of flutter vs. Λ.

Compressible Flow

The inclusion of fluid compressibility affects significantly the web aerodynamic stability. This effect can in principle be investigated using as similar approach using ANSYS as described for the incompressible fluid. However, a key difference is that infinite boundary elements will need to be used to capture the effect of radiation damping in the farfield. However the effects on web stability of the fluid compressibility can be deduced without resorting to FEM computations.

Indeed, it is well known that the inclusion of compressibility introduces in addition to the added inertia, an added radiation damping matrix [20]. This in turn adds a positive definite symmetric damping matrix C to the discretized web equations. At the critical speed the K matrix loses positive definiteness but soon restabilizes gyroscopically. The Kelvin Tait Chetaev theorem states that the addition of the slightest positive definite damping to a gyroscopically stabilized system with non-positive K, will destabilize the system. Thus each mode will destabilize immediately following its gyroscopic restabilization. Instead of coupled mode flutter, flutter will occur in individual modes at speeds that are lower than the speed for coupled mode coalescence.

CONCLUSIONS

The effects of incompressible and compressible potential flow coupling to sub-critical speed web vibration and supercritical speed stability are investigated in detail. A semi-analytical method using FEM for the fluid coupling and the assumed modes method for the moving web is developed for the purpose. The main results of the study are as follows:

1. Aerodynamic coupling significantly reduces the web frequencies and spreads apart the frequencies that would be clustered together without air coupling.
2. The in-vacuo web system at super-critical speeds undergoes divergence instability, gyroscopic restabilization, and flutter of several modes within a small speed range. The superposition of these modes in can result in a complicated edge flutter motion.
3. For webs with areal density of about 1 g/m^2 or larger the incompressible fluid coupling reduces the speed of the onset of flutter and the flutter frequency. Flutter occurs by means of dual mode coalescence.
4. Compressible fluid coupling adds positive definite damping to the system and single mode instead of dual mode flutter will occur.
5. Critical speeds do not change with incompressible or with compressible fluid coupling.

Finally, we note that web coupling to a stationary surrounding potential flow predict web flutter exclusively at supercritical speeds. In many applications edge flutter is expected to occur at sub-critical speeds. In such cases it is important to consider base flows in the cross-span direction induced by web transport and fluid viscosity [10]. This is the subject of ongoing research by the authors.

REFERENCES

1. Wickert, J. A., and Mote Jr., C. D., "Current Research on the Vibration and Stability of Axially-Moving Materials," Shock and Vibration Digest, May, 1988, pp. 3-13.
2. Ulsoy, A. G., and Mote Jr., C. D., "Vibration of Wide Band-Saw Blades," ASME Journal of Engineering for Industry, Vol. 104, 1982, pp. 71-78.
3. Wang, X., "Numerical Analysis of Moving Orthotropic Thin Plates," Computers and Structures, Vol. 70, 1999, pp. 467-486.
4. Laukkanen, J., "FEM Analysis of a Travelling Web," Computers and Structures, Vol. 80, 2002, pp. 1827-1842.
5. Koivurova, H., and Pramila, A., "Nonlinear Vibration of Axially Moving Membrane by Finite Element Method," Computational Mechanics, Vol. 20, 1997, pp. 573-581.
6. Mockensturm, E. M., and Mote Jr., C. D., "Steady Motions of Translating, Twisted Webs," International Journal of Non-Linear Mechanics, Vol. 34, 1999, pp. 247-257.
7. Guo, C. Q., and Paidoussis, M. P., "Stability of Rectangular Plates with Free Side-Edges in Two-Dimensional Inviscid Channel Flow," Journal of Applied Mechanics – Transactions of the ASME, Vol. 67, No. 1, 2000, pp. 171-176.
8. Chang, Y. B., and Moretti, P. M., "An Experimental Study on Edge Flutter in Webs," Applied Mechanics Division - Proceedings of the ASME, Vol. 149, 1992.

9. Chang, Y. B., Cho, H. C., and Moretti, P. M., "Edge Flutter," Noise Control and Acoustics Division - Proceedings of the ASME, Vol. 26, 1999, pp. 413-423.
10. Chang, Y. B., and Moretti, P. M., "Flow-Induced Vibration of Free Edges of Thin Films," Journal of Fluids and Structures, Vol. 16, No. 7, 2002, pp. 989-1008.
11. Watanabe, Y., Suzuki, S., Sugihara, M., and Sueoka, Y., "An Experimental Study of Paper Flutter," Journal of Fluids and Structures, Vol. 16, No. 4, 2002, pp. 529-542.
12. Watanabe, Y., Isogai, K., Suzuki, S., and Sugihara, M., "A Theoretical Study of Paper Flutter," Journal of Fluids and Structures, Vol. 16, No. 4, 2002, pp. 543-560.
13. Pramila, A., "Sheet Flutter and the Interaction between Sheet and Air," Tappi Journal, 1986, pp. 70-74.
14. Pramila, A., "Natural Frequencies of a Submerged Axially Moving Band," Journal of Sound and Vibration, Vol. 113, 1987, pp. 198-203.
15. Wang, X., "Finite Element Analysis of Air-Sheet Interactions and Flutter Suppression Devices," Computers and Structures, Vol. 64, No. 5/6, 1997, pp. 983-994.
16. Niemi, J., and Pramila, A., "FEM-Analysis of Transverse Vibrations of an Axially Moving Membrane Immersed in Ideal Fluid," International Journal for Numerical Methods in Engineering, Vol. 24, 1987, pp. 2301-2313.
17. Raman, A., Wolf, K. D., and Hagedorn, P., "Observations on the Vibrations of Paper Webs," Proceeding of the International Conference on Web Handling, Stillwater, OK, 2001.
18. Turnbull, P. F., Perkins, N. C., and Schultz, W. W., "Contact-Induced Nonlinearity in Oscillating Belts and Webs," Journal of Vibration and Control, Vol. 1, 1995, pp. 459-479.
19. Meirovitch, L., Principles and Techniques of Vibrations, Prentice-Hall, New Jersey, 1997, pp. 542-543.
20. Fahy, F., Sound and Structrual Vibration – Radiation, Transmission, and Response, Academic Press, London, 2000.